Chapter 8

Clustering of i_{775} dropout galaxies at $z \sim 6$ in GOODS and the UDF

Abstract. We measured the angular clustering among a sample of 506 i_{775} dropout galaxies obtained from deep ACS fields to study clustering at $z \sim 6$. For our largest and most complete subsample ($L \gtrsim 0.5L^*_{z=6}$), we detected clustering at $\sim 94\%$ significance. We derive a (co-moving) spatial correlation length of $r_0 = 3.6^{+1.7}_{-2.5}\ h_{72}^{-1}$ Mpc and bias $b = 3.6^{+1.3}_{-2.2}$, using an accurate model for the redshift distribution. No clustering could be detected in the much deeper but significantly smaller UDF sample. We compare our findings to Lyman break galaxies at $z \sim 3-5$ at a fixed luminosity. Our best estimate of the bias parameter implies that i_{775} dropouts are hosted by dark matter halos having masses of $\sim 10^{11}\ M_\odot$, consistent with the typical mass of halos hosting V_{606} dropouts at $z \sim 5$. We evaluate a recent claim by Lee et al. (2005) that at $z \gtrsim 5$ star formation might have occurred more efficiently compared to that at $z = 3-4$. This may provide an explanation for the very mild evolution observed in the rest frame UV luminosity density between $z = 6$ and 3. Although our results are consistent with the star formation efficiency also being higher at $z \sim 6$, our errors are too large to find conclusive evidence for this.

R. A. Overzier, R. J. Bouwens, G. D. Illingworth & M. Franx
Submitted to *The Astrophysical Journal Letters*

8.1 Introduction

The Advanced Camera for Surveys (ACS, Ford et al. 1998) aboard the *Hubble Space Telescope* has made the detection of star-forming galaxies at $z \sim 6$ (i_{775} dropouts) relatively easy. The largest sample of i_{775} dropouts currently available (Bouwens et al. 2006) comes from the Great Observatories Origins Deep Survey (GOODS, Giavalisco et al. 2004), allowing the first quantitative analysis of galaxies only 0.9 Gyr after recombination[1] (Stanway et al. 2003; Bouwens et al. 2003; Yan & Windhorst 2004; Dickinson et al. 2004; Malhotra et al. 2005,see also Shimasaku et al. 2005; Ouchi et al. 2005). Bouwens et al. (2006) found evidence for strong evolution of the luminosity function between $z \sim 6$ and 3, while the (unextincted) luminosity density at $z \sim 6$ is only $\sim 0.8\times$ lower than that at $z \sim 3$. Some i_{775} dropouts have significant Balmer breaks, indicative of stellar populations of >100 Myr in age and masses comparable to those of present-day L^* galaxies (Eyles et al. 2005; Yan et al. 2005). These i_{775} dropouts may end up as relatively red galaxies at $z = 2 - 4$ (Franx et al. 2003).

Through the study of the clustering we can address fundamental cosmological issues that cannot be answered from the study of galaxy light alone. The strength of clustering and its evolution with redshift relates to the bias of galaxies, relative to the underlying dark matter. The two-point angular correlation function (ACF) has been used to measure the clustering of Lyman break galaxies (LBGs) at $z = 3 - 5$ (e.g. Adelberger et al. 1998; Arnouts et al. 1999; Magliocchetti & Maddox 1999; Giavalisco & Dickinson 2001; Ouchi et al. 2001; Arnouts et al. 2002; Porciani & Giavalisco 2002; Ouchi et al. 2004; Adelberger et al. 2005; Hildebrandt et al. 2005; Allen et al. 2005; Kashikawa et al. 2006). These studies have found that LBGs are highly biased with respect to the dark matter ($b \simeq 2 - 8$), and that this biasing depends strongly on rest frame UV luminosity, as well as, to a lesser extent, on dust and redshift. Recently, using both wide and deep surveys, the clustering statistics of LBGs have reached the level of sophistication at which one can measure two physically different contributions. At small angular scales the ACF is dominated by the highly non-linear clustering of galaxies within single dark matter halos, whereas at large scales its amplitude tends to the 'classical' clustering of galaxies residing in different halos (Ouchi et al. 2005a; Lee et al. 2005), as explained by the framework of the halo occupation distribution (e.g. Zehavi et al. 2004; Hamana et al. 2004). A detailed understanding of the clustering properties of galaxies at $z \sim 6$ is also important for the interpretation of overdensities recently observed towards luminous $z \sim 6$ quasars and in the field (Ouchi et al. 2005; Stiavelli et al. 2005; Wang et al. 2005; Zheng et al. 2006). These overdensities may demarcate structures that preceeded the present-day massive galaxies and clusters (Springel et al. 2005). Our aim here is to 'complete' the census of clustering to $z \sim 6$ as follows. In Sections 2 and 3 we describe the sample, and present our measurements of the ACF. In Section 4 we derive cosmological quantities, and discuss our findings.

[1] Throughout this letter we use a cosmology $[\Omega_M, \Omega_\Lambda, h_{72}, n, \sigma_8]$=[0.27,0.73,1.0,1.0,0.9] with $H_0 = 72\, h_{72}$ km s^{-1} Mpc^{-1}.

8.2 Data

The present analysis is based on the sample of i_{775} dropouts described in detail by Bouwens et al. (2006). We used the ACS data from the GOODS v1.0 release, which was processed together with a substantial amount of overlapping pointings that have since become available, i.e., the Ultra Deep Field (UDF) parallel fields (Thompson et al. 2005), Galaxy Evolution from Morphology and Spectral energy distributions (GEMS; Rix et al. 2004), and supernovae search data (Riess et al., Perlmutter et al., in preparation), using 'Apsis' (Blakeslee et al. 2003). The 10σ detection limit was 27.5 in z_{850} in a $0\farcs2$ diameter aperture. We also used a deep sample of i_{775} dropouts selected from the UDF (Beckwith et al., in preparation), which had a 10σ detection limit of 29.2. The final areas are listed in Table 8.1. The i_{775}-dropout distribution in the GOODS fields is shown in Fig. 8.1.

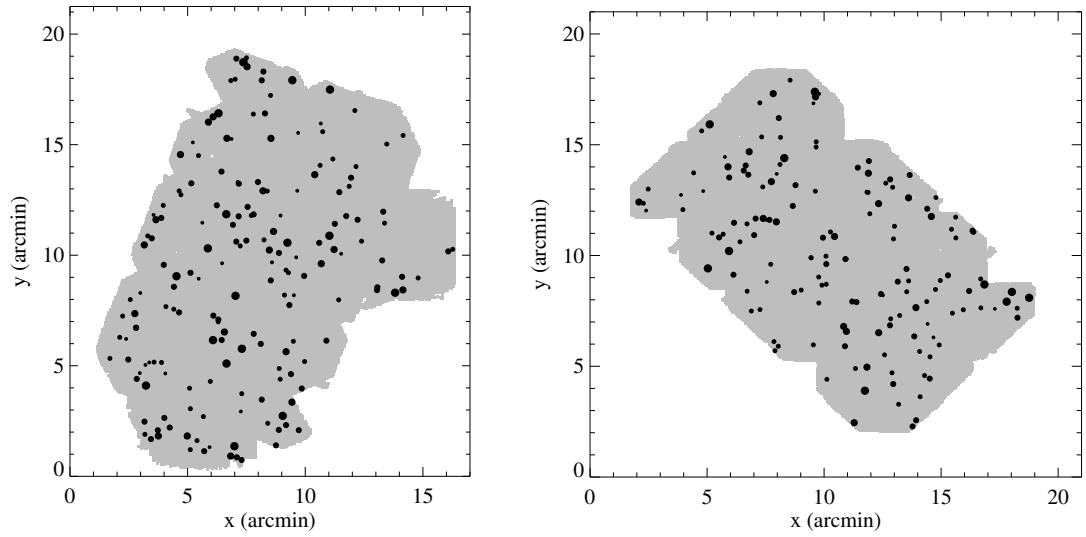

Figure 8.1 — The distributions of i_{775}-dropouts in the GOODS CDFS (left panel) and HDFN (right panel) fields.

Objects were selected by requiring (i_{775}–z_{850})>1.3, and (V_{606}–z_{850})>2.8 or non-detections (<2σ) in V_{606} to exclude lower redshift interlopers. Point sources were removed based on high stellarity parameters >0.75. The estimated remaining contamination due to photometric scatter, red interlopers, and stars is ∼7% to z_{850}=28.0, of which 2% is due to stars (see Bouwens et al. (2006) for details). The effective redshift distributions for GOODS and the UDF are shown in Fig. 8.2. The effective rest frame UV luminosity of the sample is $L \approx 0.5L^*_{z=6}$ for z_{850}∼27.5 (Bouwens et al. 2006). Note that the luminosity is quite sensitive to redshift due to forest attenuation entering z_{850} at $z > 6$, with $L^*_{z=6}$ corresponding to z_{850}∼26.5 (∼28) at $z = 5.5$ ($z = 6.5$).

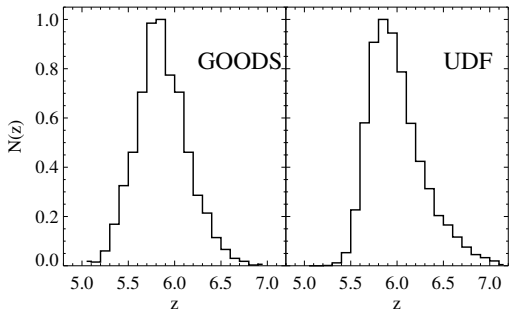

Figure 8.2 — The redshift distributions of i_{775} dropouts in our GOODS (left panel) and UDF (right panel) selections (estimated by projecting a complete UDF B_{435} dropout sample scaled to the sizes and colors as found for the i_{775} dropout sample to $z \sim 5-7$, see Bouwens et al. (2006) for details). As a result of a more significant photometric scatter in (i_{775}–z_{850}), the selection extends to lower redshifts in GOODS than it does for the UDF.

8.3 The angular correlation function

We measured the ACF, $w(\theta)$, defined as the excess probability of finding two sources in the solid angles $\delta\Omega_1$ and $\delta\Omega_2$ separated by the angle θ, over that expected for a random Poissonian distribution (Peebles 1980). We used the estimator $w(\theta) = [DD(\theta) - 2DR(\theta) + RR(\theta)]/RR(\theta)$ of Landy & Szalay (1993), where $DD(\theta)$, $DR(\theta)$ and $RR(\theta)$ are the number of pairs of sources with angular separations between θ and $\theta+\Delta\theta$ measured in the data, random, and data-random cross catalogs, respectively. We used 16 random catalogs containing ∼100× more sources than the data catalog of

similar angular geometry. Errors on $w(\theta)$ were bootstrapped (Ling et al. 1986). We assumed a power-law ACF of the form $w(\theta)=A_w\theta^{-\beta}$ and determined its amplitude, A_w, by fitting the function $w(\theta)=A_w\theta^{-\beta}-IC$. The integral constraint ($IC=\int\int w(\theta)d\Omega_1 d\Omega_2/\Omega^2$, where Ω is the survey area) was $0.033A_w$ for GOODS, and $0.074A_w$ for the UDF. We did not attempt to fit the slope of the ACF and assumed $\beta = 0.6$ based on the results of Lee et al. (2005). The ACF was fitted over the range 10″–300″ (10″–200″ for the UDF), corresponding to roughly 0.4–10 h_{72}^{-1} Mpc comoving at $z \sim 6$. The lower value of 10″ is larger than the virial radius of a 10^{12} $M_\odot$ halo to ensure that we are measuring the large-scale clustering (and not receiving a contribution at small scales from the sub-halo component). Because the results of the fits are sensitive to the size of the bins used, we determined the amplitude and its error from Monte Carlo simulations. Each datapoint was randomly varied according to a normal distribution with standard deviation equal to its bootstrap error, and the bin size was varied within the range 5″–50″. The final amplitude and the error are the mean and standard deviations among the fits that had $A_w > 0$. We note that if the 7% of contamination in the sample has a uniform distribution, the measured amplitude should be multiplied by ∼1.16 to yield the corrected clustering amplitude.

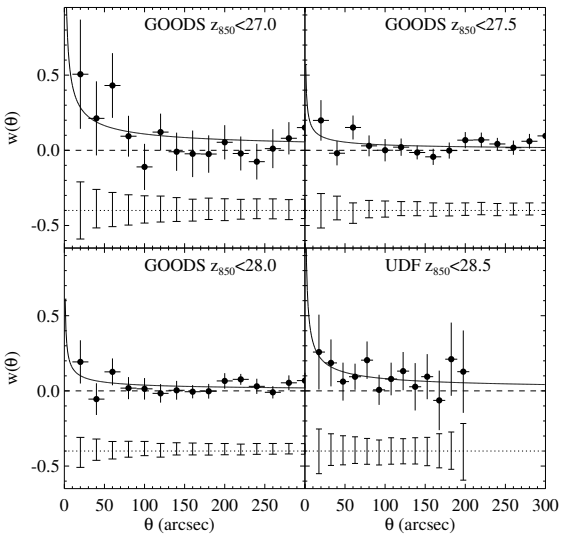

Figure 8.3 — The ACF of i_{775} dropouts from GOODS and the UDF. Points indicate the measurements corrected using the integral constraint for GOODS with z_{850}<27 (top left), z_{850}<27.5 (top right) and z_{850}<28 (bottom left), and for the UDF with z_{850}<28.5 (bottom right). Errors (1σ) were bootstrapped. The best-fit power-laws were obtained through Monte Carlo simulations of the measurements at $\theta > 10''$ (lines). The mean and standard deviations among 1000 Poissonian distributions are indicated by the empty error bars, offset by –0.4 in the vertical direction for clarity. In the UDF, the measurements become very uncertain at $\theta \gtrsim 200''$ since we are reaching the approximate angular extent of that field.

8.3.1 Results from GOODS

Fig. 8.3 shows the ACF in GOODS for various limiting z_{850}-magnitudes. The fit results are given in Table 8.1. A positive signal was measured out to $\theta \sim 50'' - 100''$, most notably among the 172 i_{775} dropouts in the z_{850}<27.0 sample, which had a best-fit amplitude of $A_w = 1.7 \pm 1.2$. For the fainter samples we found $A_w \approx 0.6 \pm 0.5$. Because the objects were selected from data of uniform depth, any signal in the ACF is unlikely to be caused by instrumental variations in the object surface density. Given the large errors on A_w, it is useful to ask whether the $w(\theta)$ observed at $\theta \lesssim 1'$ could be the result of shot noise in a random object distribution. We created 1000 random distributions with the same geometry and the same number of points as our data, and calculated the ACF in each of the random samples. The mean and standard deviation at each θ is plotted in Fig. 8.3 (offset by –0.4). We calculate the chance of reproducing the observed clustering in the random realizations, using the average $w(\theta)$ measured over the first four bins ($\theta < 100''$) as a gauge of this clustering. We find a chance of 0.1% for the z_{850}<27.0 sample. The random occurrences are respectively 6% and 11% for the fainter samples.

Another test of the measured clustering was as follows. We used the formalism of Soneira & Peebles (1978) to create mock samples with a choice ACF in two dimensions. A $250' \times 250'$ mock field with similar surface density

as the i_{775} dropouts allowed us to mimick the measured A_w to an accuracy of 98%, determined from a fit. Next, we randomly extracted 100 mock 'GOODS' surveys and measured the mean $w(\theta)$ and its standard deviation using identical binning and fitting as for the real sample. Fig. 8.4 demonstrates that the amplitude of the observed $w(\theta)$ at $\theta \lesssim 1'$ lies within $\lesssim 1\sigma$ of the expected amplitudes for our model ACF, but also illustrates the large scatter in the extracted amplitudes due to the small sample size (shaded region in Fig. 8.4).

In the above analysis we restricted ourselves to clustering at $\theta \geq 10''$. Our measurements also showed an excess of pair counts at $\theta < 10''$. Upon closer inspection it was found that the excess was strictly limited to $\theta < 5''$, with $w(2\farcs5) \sim 2.0 \pm 0.9$. The excess is consistent with an enhancement of $w(\theta)$ due to sub-halo clustering (Ouchi et al. 2005; Lee et al. 2005) to 1.7σ confidence, but the exact amplitude cannot be determined accurately due to the small number of pairs (11 pairs at $z_{850} < 28.0$). A similar small-scale excess was found by Shimasaku et al. (2006) in the distribution of Lyα emitters at $z = 5.7$.

8.3.2 Results from the UDF

The analysis is hampered by the relatively small number of sources available, owing to its $\sim 30\times$ smaller area compared to GOODS, although its greater depth (1.5 mag) partially makes up for this lack of area. Fig. 8.3 (bottom right) shows the ACF obtained from the 52 i_{775} dropouts in our $z_{850} < 28.5$ UDF sample. The best-fit amplitude is $A_w = 1.3 \pm 1.2$. The $z_{850} < 29.0$ sample containing 95 objects gave a best-fit $A_w = 0.3 \pm 0.5$. As with GOODS, we created 1000 random 'UDF' fields to measure the effect of shot noise. The results are indicated again in the bottom right panel of Fig. 8.3. In about 13% of the random fields, $w(\theta)$ was equal to or greater than the $w(\theta)$ measured at $\theta < 1'$. The relatively large error and the small amplitude of our faintest UDF sample is likely the result of the small sample size and the strong luminosity dependence of clustering observed at lower redshifts (e.g. Kashikawa et al. 2006).

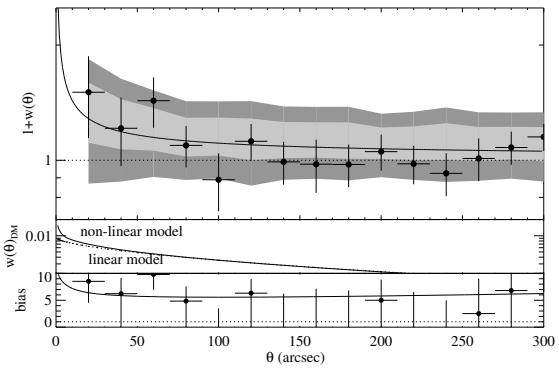

Figure 8.4 — The ACF and bias for the $z_{850} < 27$ sample. The top panel shows the clustering measurements (points), and the best-fit $w(\theta)$ (solid line). The shaded region indicates the range found among 100 mock samples extracted from a $250' \times 250'$ field with a built-in clustering amplitude as measured for the $z_{850} < 27$ sample at 1σ (light grey) and 2σ (dark grey). The middle panel shows the non-linear clustering of dark matter (Peacock & Dodds 1996), where the linear case has been indicated to illustrate the additional power at small θ in the non-linear model. The redshift distribution of Fig. 8.2 was used for Limber inversion of the dark matter clustering. The bottom panel shows the bias as a function of θ (points) and the bias for the best-fit ACF (solid line).

8.4 Derivation of cosmological quantities

While the uncertainties are large, our measurements can nevertheless be used to estimate the spatial correlation length, r_0, and bias, b, given the redshift selection functions (Fig. 8.2). We used the cosmological Limber equation adopted for our cosmology to invert A_w to obtain r_0 (Table 8.1). The clustering was assumed to be fixed in comoving coordinates across the redshift selection window. We found $r_0 \sim 4 \pm 2\ h_{72}^{-1}$ Mpc for the $z_{850} < 27.5$ and $z_{850} < 28$ samples. At $z_{850} < 27$, the best-fit value was $r_0 = 7.2^{+2.8}_{-3.7}\ h_{72}^{-1}$ Mpc, consistent with the fainter subsamples within the errors. These correlation lengths increase by ~ 10 percent if we apply the contamination correction derived in Section 3. Also, it is important to realise that except for the brightest sample, the samples are not independent. Therefore, if the brightest subsample is more strongly clustered, then the fainter samples must be more weakly clustered to yield the measured r_0.

We calculated the galaxy-dark matter bias, defined as $b(\theta) \equiv \sqrt{w(\theta)/w_{dm}(\theta)}$, where $w_{dm}(\theta)$ is the ACF of the dark matter as 'seen' through our redshift selection window. $w_{dm}(\theta)$ was calculated using the non-linear fitting function of Peacock & Dodds (1996) (middle panel of Fig. 8.4). In the bottom panel of Fig. 8.4 we have indicated the bias as a function of θ (points). Our best-fit ACF implies $b(\theta{\sim}30'')=6.2^{+1.8}_{-2.7}$ (solid line), with $b{\sim}4-5$ for the fainter samples. Applying the contamination correction yields values that are ∼5 percent higher.

It is important to evaluate how our results might be influenced by cosmic variance. For GOODS we estimate $\sigma_v{\sim}0.1$–0.2, while $\sigma_v{\sim}0.5$ for the UDF (σ_v being the square root of the cosmic variance), assuming a one-to-one correspondence between dark halos and galaxies as in Somerville et al. (2004). This shows that the GOODS i_{775} dropout sample is likely to be a fairly representative sample, while the UDF results may suffer significantly from the relatively small effective volume. For the UDF, the uncertainty on r_0 due to cosmic variance is likely of similar order of magnitude as the uncertainty in our current measurements. The small cosmic variance derived for GOODS indicates that for these fields, our results are dominated by the uncertainty in the measurements alone. While it is possible that the positive signal out to $\sim 1'$ is the result of strong sub-halo clustering (see Lee et al. 2005; Ouchi et al. 2005), the occurrence of such halos becomes increasingly rare with redshift and by limiting the fits to $\theta \gtrsim 10''$ we have suppressed the dominant contribution from sub-halo clustering.

We can directly compare our results to measurements performed by Lee et al. (2005) who found $b{\sim}3.3{\pm}0.5$ for faint V_{606} dropouts ($z \sim 5$) also from GOODS. At $z_{850}{\sim}27.5$ we probe approximately the same rest frame luminosity ($M_z \lesssim -19.5$) as their faintest (i.e. $z_{850}{\leq}27$) V_{606} dropout sample. To this limit, we measure a bias of $b = 3.6^{+1.3}_{-2.2}$, which suggests an average halo mass in the (1σ) range $\sim 1\times10^{10} - 3\times10^{11}$ $M_\odot$, assuming that the bias of the i_{775} dropouts corresponds to that of dark halos more massive than the average halo hosting them (Sheth & Tormen 1999). This range is similar to the average halo mass of V_{606} dropouts. Interestingly, Lee et al. (2005) found that at slightly higher rest frame luminosities ($M_z \lesssim -20$), the clustering of V_{606} dropouts is incompatible with that of U and B_{435} dropouts at $z = 3-4$, for which much stronger clustering is found and correspondingly a $\sim 10\times$ larger halo mass ($\sim 10^{12}$ $M_\odot$) is inferred, as shown in Fig. 8.5. Can we confirm this result using our brightest ($M_z \lesssim -20$) GOODS sample? The bias for this sample implies halo masses in the range $M \sim 5\times10^{10} - 2\times10^{12}$ $M_\odot$. Although our best values for r_0 and b are almost twice as high as for our fainter sample, the difference cannot be regarded as statistically significant. Focusing instead on the $z_{850}< 27.5$ sample (which is our best estimate of the clustering of i_{775} dropouts given the large sample size and large relative completeness), the inferred halo mass is lower than that at $z = 4$ only at $\sim 1\sigma$ significance, owing to the relatively large error

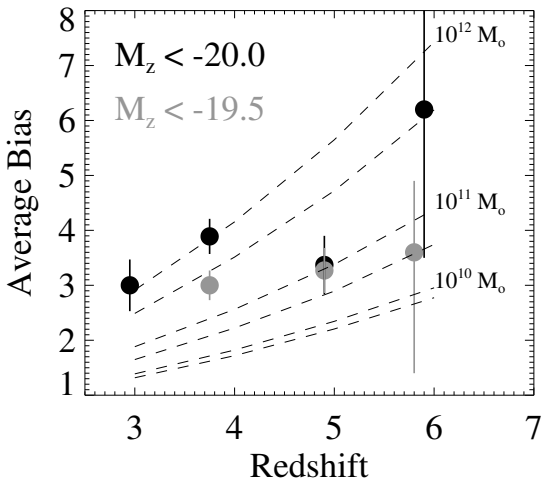

Figure 8.5 — Bias parameters of U, B_{435}, and V_{606}-dropouts as measured by Lee et al. (2005), compared to the bias estimated for the i_{775}-dropouts. Our best estimate for the halo mass at $z \sim 6$ is $\sim 10^{11}$ $M_\odot$, albeit with large errors. The estimate of the halo mass of the brightest ($M_z < -20$) V_{606}-dropouts at $z = 5$ is $\sim 10\times$ lower than that of B_{435}-dropouts at $z = 4$, but the errors at $z \sim 6$ are too large to conclude that this is generally true for luminous star-forming galaxies at $z \simeq 5-6$.

Table 8.1 — ACF and related physical quantities.

Sample	Area (arcmin^2)	N	A_w	r_0 (h_{72}^{-1} Mpc)	$b(30'')$
enhanced GOODS data					
<27.0	$320^\dagger$	172	1.72 ± 1.17	$7.2^{+2.8}_{-3.7}$	$6.2^{+1.8}_{-2.7}$
<27.5	$320^\dagger$	293	0.57 ± 0.49	$3.6^{+1.7}_{-2.5}$	$3.6^{+1.3}_{-2.2}$
<28.0	$320^\dagger$	331	0.61 ± 0.41	$3.8^{+1.4}_{-1.9}$	$3.7^{+1.1}_{-1.6}$
UDF data					
<28.5	$11^\dagger$	52	1.29 ± 1.22	$5.9^{+3.0}_{-4.9}$	$5.4^{+2.1}_{-4.1}$
<29.0	$11^\dagger$	95	0.29 ± 0.47	< 4.2	< 4.1

† Approximate areal coverage with the 10σ detection limit.

as well as to the fact that the decrease in the effective halo mass from $z = 4$ to 5 at these luminosities is not as dramatic as observed at luminosities of $M_z \lesssim -20$.

Lee et al. (2005) argued that star formation may have occurred more efficiently at higher redshifts ($z \sim 5$) than it did at $z \sim 3 - 4$, given that objects of comparable luminosity are found in less massive halos at $z \sim 5$. If this is true (and can be confirmed for galaxies at $z \gtrsim 6$), it would largely offset changes that are occurring in the mass function over this range. As such, this may provide at least a partial explanation for the mild evolution in the luminosity density from $z = 6$ to 3 (Bouwens et al. 2006).

In conclusion, we used the largest available sample of i_{775} dropouts to study clustering at $z \sim 6$. We found a small signal, although its amplitude is not well constrained due to the large errors on the individual datapoints. The present analysis is reminiscent of that performed at $z \sim 3 - 5$ based on the original Hubble Deep Fields. The clustering of galaxies at $z \sim 6$ will continue to be studied from large samples of relatively bright LBGs, as well as Lyα emitters selected using groundbased surveys of deep and wide fields (see e.g., Shimasaku et al. 2005, 2006). Although it might become possible in the near future to increase our sample size by a factor of $\sim 2 - 3$ by relaxing our current i_{775} dropout detection threshold, to perform an analysis at the same level of detail as currently performed at $z \sim 5$ would require another six GOODS fields, for $\sim$1200 arcmin^2 in total.

Acknowledgments

RAO is grateful for helpful discussions with Peter Katgert and Huub Röttgering, and the referee, Masami Ouchi, for his many good suggestions. ACS was developed under NASA contract NAS 5-32865, and this research has been supported by NASA grant NAG5-7697.

References

Adelberger, K. L., Steidel, C. C., Giavalisco, M., Dickinson, M., Pettini, M., & Kellogg, M. 1998, ApJ, 505, 18
Adelberger, K. L., Steidel, C. C., Pettini, M., Shapley, A. E., Reddy, N. A., & Erb, D. K. 2005, ApJ, 619, 697
Allen, P. D., Moustakas, L. A., Dalton, G., MacDonald, E., Blake, C., Clewley, L., Heymans, C., & Wegner, G. 2005, MNRAS, 360, 1244
Arnouts, S., Cristiani, S., Moscardini, L., Matarrese, S., Lucchin, F., Fontana, A., & Giallongo, E. 1999, MNRAS, 310, 540
Arnouts, S. et al. 2002, MNRAS, 329, 355
Blakeslee, J. P., Anderson, K. R., Meurer, G. R., Benítez, N., & Magee, D. 2003, in ASP Conf. Ser. 295: Astronomical Data Analysis Software and Systems XII, 257
Bouwens, R., Broadhurst, T., & Illingworth, G. 2003, ApJ, 593, 640
Bouwens, R. J., Illingworth, G. D., Blakeslee, J. P., & Franx, M. 2006, ApJ, In Press (astro-ph/0509641)
Dickinson, M. et al. 2004, ApJ, 600, L99
Eyles, L. P., Bunker, A. J., Stanway, E. R., Lacy, M., Ellis, R. S., & Doherty, M. 2005, MNRAS, 364, 443
Ford, H. C. et al. 1998, in Proc. SPIE Vol. 3356, p. 234-248, Space Telescopes and Instruments V, Pierre Y. Bely; James B. Breckinridge; Eds., 234–248

Franx, M., et al. 2003, ApJ, 587, L79
Giavalisco, M., & Dickinson, M. 2001, ApJ, 550, 177
Giavalisco, M. et al. 2004, ApJ, 600, L93
Hamana, T., Ouchi, M., Shimasaku, K., Kayo, I., & Suto, Y. 2004, MNRAS, 347, 813
Hildebrandt, H. et al. 2005, A&A, 441, 905
Kashikawa, N. et al. 2006, ApJ, 637, 631
Landy, S. D., & Szalay, A. S. 1993, ApJ, 412, 64
Lee, K.-S., Giavalisco, M., Gnedin, O., Somerville, R., Ferguson, H., Dickinson, M. E., & Ouchi, M. 2006, ApJ, In Press (astro-ph/0508090)
Ling, E. N., Barrow, J. D., & Frenk, C. S. 1986, MNRAS, 223, 21P
Magliocchetti, M., & Maddox, S. J. 1999, MNRAS, 306, 988
Malhotra, S., et al. 2005, ApJ, 626, 666
Ouchi, M., et al. 2001, ApJ, 558, L83
Ouchi, M. et al. 2005a, ApJ, 635, L117
—. 2005b, ApJ, 620, L1
—. 2004, ApJ, 611, 685
Peacock, J. A., & Dodds, S. J. 1996, MNRAS, 280, L19
Peebles, P. J. E. 1980, The large-scale structure of the universe (Princeton University Press, 1980. 435 p.)
Porciani, C., & Giavalisco, M. 2002, ApJ, 565, 24
Rix, H.-W. et al. 2004, ApJ, 152, 163
Sheth, R. K., & Tormen, G. 1999, MNRAS, 308, 119
Shimasaku, K., Ouchi, M., Furusawa, H., Yoshida, M., Kashikawa, N., & Okamura, S. 2005, PASJ, 57, 447
Shimasaku, K. et al. 2006, PASJ, In Press (astro-ph/0602614)
Somerville, R. S., Lee, K., Ferguson, H. C., Gardner, J. P., Moustakas, L. A., & Giavalisco, M. 2004, ApJ, 600, L171
Soneira, R. M., & Peebles, P. J. E. 1978, AJ, 83, 845
Springel, V. et al. 2005, Nature, 435, 629
Stanway, E. R., Bunker, A. J., & McMahon, R. G. 2003, MNRAS, 342, 439
Stiavelli, M. et al. 2005, ApJ, 622, L1
Thompson, R. I. et al. 2005, AJ, 130, 1
Wang, J. X., Malhotra, S., & Rhoads, J. E. 2005, ApJ, 622, L77
Yan, H. et al. 2005, ApJ, 634, 109
Yan, H., & Windhorst, R. A. 2004, ApJ, 612, L93
Zehavi, I. et al. 2004, ApJ, 608, 16
Zheng, W. et al. 2006, ApJ, 640, 574